Particle-Induced Bit Errors in High Performance Fiber Optic Data Links for Satellite Data Management

Paul W. Marshall[1,2], Cheryl J. Dale[1], Martin A. Carts[1,2], and Kenneth A. LaBel[3]

1 Naval Research Laboratory, Washington, DC, 20375
2 SFA, Inc., Landover, MD, 20785
3 NASA Goddard Space Flight Center, Greenbelt, MD, 20771

Abstract

Experimental test methods and analysis tools are demonstrated to assess particle-induced bit errors on fiber optic link receivers for satellites. Susceptibility to direct ionization from low LET particles is quantified by analyzing proton and helium ion data as a function of particle LET. Existing single event analysis approaches are shown to apply, with appropriate modifications, to the regime of temporally (rather than spatially) distributed bits, even though the sensitivity to single events exceeds conventional memory technologies by orders of magnitude. The cross-section LET dependence follows a Weibull distribution at data rates from 200 to 1000 Mbps and at various incident optical power levels. The LET threshold for errors is shown, through both experiment and modeling, to be 0 in all cases! The error cross-section exhibits a strong inverse dependence on received optical power in the LET range where most orbital single events would occur, thus indicating that errors can be minimized by operating links with higher incident optical power. Also, an analytic model is described which incorporates the appropriate physical characteristics of the link as well as the optical and receiver electrical characteristics. Results indicate appropriate steps to assure suitable link performance even in severe particle orbits.

I. INTRODUCTION

The maturity and improved reliability of fiber optic data transmission methods now make this technology available for satellite designers to take advantage of the high data throughput, and low noise and power characteristics. For example, NASA has chosen to implement the Small Explorer Data System (SEDS) telemetry and control bus in fiber optics to provide a significantly reduced weight and power solution to spacecraft subsystem interfacing, while providing EMI/RFI immunity to the cable harness [1]. This space qualified version of the MIL-STD-1773 bus is now available for telemetry and control applications. Its successful on-orbit performance since July 1992 demonstrates the reliability of the technology. Currently there are a number of bus design efforts under way to cover a much broader range of capabilities [2]. These include the Dual Rate enhancement being developed for MIL-STD-1773 which will allow simultaneous 1 and 20 Mbps operation and thereby expand the application base to include many payload scenarios. Also, two development efforts are now under way for higher rate busses, the Boeing STAR bus for 20-400 Mbps transmission [3] and the TRW/Honeywell RING bus for 20-3200 Mbps operation [4-6]. Each of these bus designs supports up to 32 nodes and will use 1300 nm multimode components.

Considerable efforts toward understanding the long term, as well as the transient effects of radiation in earth orbits, have played a key role in space qualifying systems such as the NASA SEDS bus [7]. In a recent review of radiation effects in fiber optic data links for satellites [8], a case was made that radiation-induced attenuation in optical fibers and displacement damage in optoelectronic sources and detectors are sufficiently well understood to enable selection of reliable components. However, the impact of single particle transients on the bit-error-ratio (BER), defined as the probability of a bit being received incorrectly, continues to be a concern [7,9,10].

This paper summarizes our understanding of the impact of single ionizing particle effects on links operating with data rates from 20 Mbps up to the Gbps range. Here we describe results of in-situ experiments in which operating fiber bus components are subjected

0018-9499/94$04.00 © 1994 IEEE

to proton and helium ion bombardment. Test results allow examination of variables such as particle energy, flux, angle of incidence, data rate, and optical signal level. By combining predicted trapped particle orbital environmental data, including spacecraft shielding effects, with system response under test, we outline an approach to predict BER in orbit and offer this as a basis for evaluating proposed hardening solutions. Such studies are critical to the design of reliable fiber optic data links for satellites.

II. Physical Mechanisms

A. *Particle Effects in Receivers*

This section examines the manner in which digital data is transmitted via a fiber optic connection and describes how particle-induced signals can disrupt data. As we have previously reported [7, 9, 10], there is compelling evidence that a fiber optic link's most sensitive component to single particle effects is the receiver photodiode. This is perhaps not so surprising in view of the fact that this optoelectronic detector functions to capture digital information at rates into the Gbps regime from optical signals with average powers of a few μW. Also, the photodiode must necessarily be large enough to capture the optical signal. For typical multimode fiber, this corresponds to surface areas of thousands of square microns (the device examined in our study has a 75 micron optical aperture with an 80 micron diameter junction). Photodiode physical cross-sections can easily exceed 10^{-5} cm^2, and owing to the extreme sensitivity, the error cross-sections can be correspondingly large.

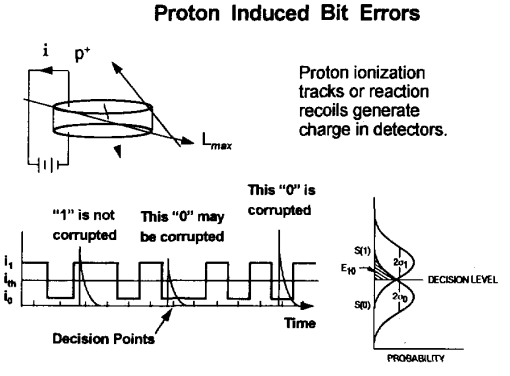

Figure 1. Proton ionization in receiver photodiodes induces photocurrents which may disrupt data.

Figure 1 depicts the disk-shaped planar photodiode structure under reverse bias conditions and indicates various particle trajectories which deposit charge by direct ionization. The sketch beneath shows resulting current pulses sensed in the receiver circuit which decay with an RC time constant determined by the circuit bandwidth. Also depicted is the received no-return-to-zero (NRZ) signal containing the digital information. The ratio between the high and low current levels, the extinction ratio, is typically about 10. Receiver circuits are almost always designed to accommodate a range of incident average optical powers and automatically adjust the decision level, or threshold, to be midway between the high and low levels. As suggested in the figure, data can be disrupted if ion-induced current exceeding the threshold current is sensed at the critical mid-bit decision when a "0" is being transmitted.

The two distributions shown at the lower right of the figure indicate the contributions of multiple noise sources leading to a distribution of signals received to represent "1s" and "0s". Except for very low incident optical signals, the shape is approximately gaussian, though the widths have been exaggerated in the sketch. According to communications decision theory, we would expect a usually small but finite probability of false bits from the intersymbol interference where the distribution tails extend beyond the decision level. Thus *any* ion-induced photocurrent flowing when a "0" has been transmitted increases the probability of false detection, and this statistical aspect must be treated as an integral part of the estimation of ion-induced errors [4]. This issue, and the points preceding it, will be revisited later in a quantitative sense when we discuss an analytic model for predicting bit errors.

Though the photodiode must be large enough to capture the optical signal, it obviously should be no larger. Our analysis indicates better SEE characteristics for III-V direct bandgap detectors since the depletion depth need only be about 2-3 microns for > 80% quantum efficiency. In contrast with indirect bandgap detectors such as Si for 830 nm applications in which depletion depths are about 20 x larger, the thinner structure minimizes both the "target" size for ion strikes as well as the ion pathlength when hit. Also, the III-V device is characteristic of the design choices being considered for high bandwidth data busses since the thin junction offers minimal capacitance. To take advantage of these benefits, each of the design efforts sited in the

introduction will use III-V InGaAs detectors for 1300 nm lightwave detection.

B. *Environment Evaluation*

For the purpose of discussing link performance on orbit, we will consider a severe environment based on the August 72 flare particle event as described in the CREME model [11]. We recommend an approach which parallels conventional heavy ion single event analysis in which one normally proceeds by evaluating the environment, including any shielding effects, in a manner which combines the device chord distribution with an LET distribution resulting in a distribution of charges deposited. Estimation of the incident orbital particle flux is slightly more involved for our case since we do not have a rectangular parallelepiped (RPP) geometry, and our material is neither silicon nor gallium arsenide. Having calculated and compared the resulting chord length distribution for right circular cylinder (RCC) versus RPP structures with thin aspect ratios, we conclude that it is not necessary to use the exact distribution. The recommended approach is to use a square RPP structure having the same surface area as the photodiode and thereby take advantage of already existing tools.

Similarly, based on calculations for GaAs and for $In_{.53}Ga_{.47}As$ using TRIM [12], we note that the physical densities of the two materials differ by only 6% and the LET (in energy per length) agree to within 3% for proton energies up to 150 MeV. When using GaAs to simulate InGaAs in the CREME model; however, it is important to recognize the lower ionization potential of 2.7 eV per ion pair for the narrower bandgap InGaAs alloy versus 4.21 eV/IP in GaAs. This is rather easily handled by a systematic 56% increase in the charge deposition results of the CREME calculation for GaAs, e.g. the results describing the number of particle events exceeding 10.0 fC in GaAs also applies for the number exceeding 15.6 fC in the same geometry with InGaAs.

Finally, though it is not usually important for single event upset analysis, it is necessary to examine the *LET* spectrum resulting from the *proton* flux of interest. In Figure 2 we present results of such an analysis for the August '72 flare event worst case flux described in CREME with 0 GV geomagnetic cutoff and 80 mils Al shielding. Each point on the curve corresponds to the number of particles per second exceeding the indicated charge threshold in an 80 micron diameter by 3 micron

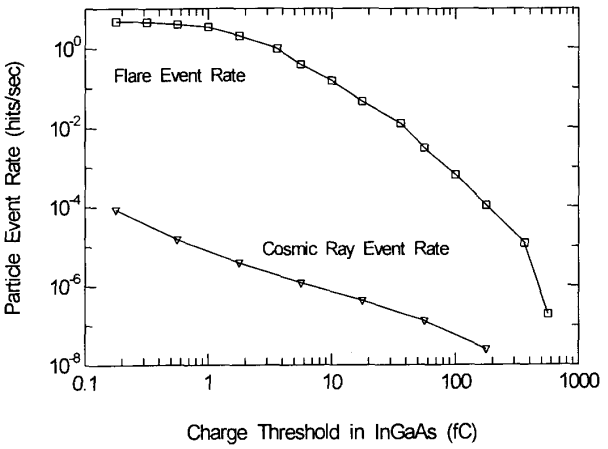

Figure 2. Particle event rates exceeding a given charge threshold are compared for the August '72 flare and galactic cosmic ray environments.

thick InGaAs structure. The 0 fC intercept of 4.8 events/s corresponds to charges of all sizes, though most of these are clearly less than 10 fC. Proton inelastic reactions are not considered, and no proton ionization events depositing more than 560 fC were possible. The solar minimum galactic cosmic ray event rates are shown for reference.

III. Experimental Approach

A commercial bit error rate test set from Broadband Communications Products, Inc. was configured to measure of link performance as shown in Figure 3.

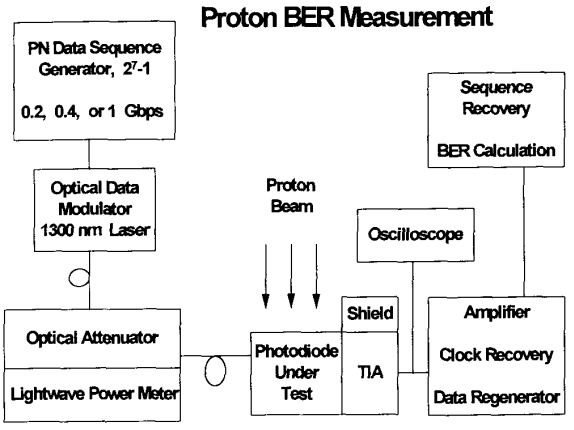

Figure 3. Commercial communications link tester modified for proton single event studies of fiber optic links to 1 Gbps.

Instrument control and data logging were accomplished using the IEEE-488 interface and LabView® by National Instruments, Inc. The tester was set to generate a serial pseudo random numeric (PN) sequence of (2^7-1) bits in length. Data rates of 200, 400, and 1000 Mbps were established by an external waveform generator. The fiber link included a programmable attenuator so that the desired optical power level could be adjusted over the range of -30 dBm to -11dBm. The optical power was monitored by an external lightwave meter or coupled onto the surface of the photodiode under test. Light was launched onto the photodiode using a 3-axis micro-manipulator stage, and coupling efficiency was maximized by tuning and monitoring the photodiode output on a digital sampling oscilloscope.

As an example of planar InGaAs detector technology, we choose the Epitaxx ETX 75 p-i-n diode which has an active optical diameter of 75 microns and a junction diameter of about 80 microns. Photodiode irradiation took place without exposing any associated circuitry, including the transimpedance amplifier. The electrical amplifier output was returned to the test set where post amplification, clock recovery, and PN pattern recognition were performed. Test set output included the BER as well as the number of errors and the percent of error free intervals down to 0.01 s. With no protons incident, a BER of 10^{-9} was measured with -27 dBm incident on the photodiode at 400 Mbps. We note that this matches the theoretical limit for the bipolar amplifier arrangement (gain=1000, 80% quantum efficiency, and 400 Mbps), and confirms that we had accurate measurement of the optical power incident to the photodiode.

With protons incident on the photodiode, we monitored the BER and the number of errors. Measurements of BER were typically made with > 100 total errors to assure good statistics. This usually covered a time interval of minutes. By logging the percent of error free intervals, we verified that for protons the errors were due to individual events and not contiguous errors from a single strike. Similarly, for higher LET He ions, we determined the average number of errors per strike using this feature.

These measurements were performed at the NRL beamline at the University of California. For in-situ measurements of data transmission with bit periods of only a few ns, one must carefully consider the beam temporal structure and its relation to the data stream. In [8], we examined the impact of the 22 MHz cyclotron frequency (at 67 MeV) which provides micro-pulses of approximately 1.3 ns duration every 44 ns. Our experiments were conducted in a manner to assure this did not influence bit-error cross-section measurements.

IV. Experiment Results and Analysis

In this section, we demonstrate how proton-induced BER effects in photodetectors can be quantified according to the well-developed tools used in more conventional single event investigations. As is customary with spatially separated arrays of memory elements in RAMs, we define bit error cross-sections for temporally separated bits in a data stream as the ratio of failed bits to the particle fluence incident on the device during the interval in which the failures are measured. Our objective is to understand the error cross-section dependence on environmental factors such as the particle energy, particle flux, and angle of incidence, each of which impact the *effective* linear energy transfer (LET). Also, for a given receiver design, we measure the cross-section dependence on the data link characteristics including the data rate and the optical power incident on the photodiode. The result is a data set which can be readily analyzed with existing descriptions of the expected environment, as described in II B, to produce high confidence estimates of link performance in orbit.

A. Angle of Incidence and Received Optical Power

To quantify the bit error cross-section dependence on two important parameters, proton angle-of-incidence and received optical power, we present the family of BER cross-section curves for 63 MeV protons on the 400 Mbps link, shown as Figure 4. Note that the cross-section at each angle is effectively reduced by increasing the incident optical power. Qualitatively, this dependence is expected since this increases the signal strength relative to a fixed impulse noise level thereby raising the receiver's decision threshold as discussed in section II. The proton trajectory with respect to the right circular cylinder effectively establishes the proton pathlength and therefore the amount of charge deposited by direct ionization. Unlike conventional heavy ion testing, we can test at high incidence angles since the 63 MeV proton has a range of about 700 mils Al.

Near minimum optical power (the noise floor is around -27 dBm for 400 Mbps), we note the 4 curves converge to cross-section values approaching the

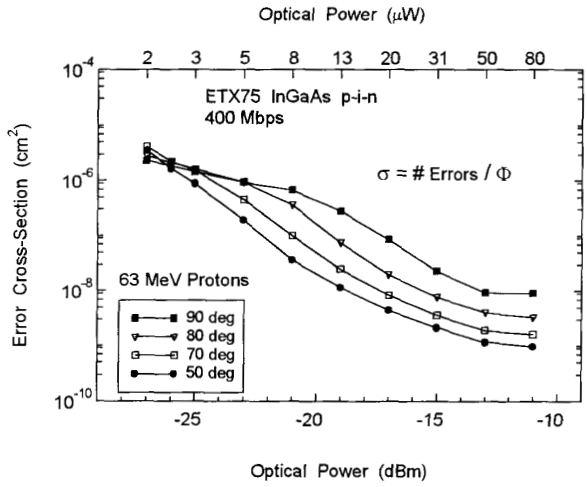

Figure 4. Proton-induced error cross-sections vary strongly with optical power and depend on particle angle.

physical dimensions of the photodiode, including effects on its projected area in the beam as it is tilted. This observed angle dependence, and the fact that we have separately determined that errors occur as singles and not multiples for protons, confirms that errors must be dominated by direct ionization rather than by less frequent nuclear reactions.

B. Cross-section versus Effective LET

The compelling evidence for the direct ionization mechanism suggests the next steps, again from heavy ion test methods. First, the data is normalized to 0 degree incidence by applying a cos(θ) correction to the fluence used in the cross-section calculation. Then we assign an *effective* LET defined as the product of the particle's LET and sec(θ). Figure 5 shows six curves describing cross-section dependence on optical power. The lower three correspond to the 50, 70 and 80 degree proton data of Figure 4, and the upper three with 18 MeV protons, then 40 and 18 MeV He ions, all at 70 degree incidence. These data reveal a strong dependence on particle LET which apparently cannot be mitigated with optical power. However, we note that the event rates for higher LET particle strikes in satellite environments are low compared to proton strikes. We also note that for the He ion data, the measured cross-section exceeds the physical dimensions, implying that single particles must be capable of causing multiple bit errors. For example, for the highest LET particle, 18 MeV He ions, we measured an average of 2.2 incorrect bits per error event at the highest data rate of 1 Gbps.

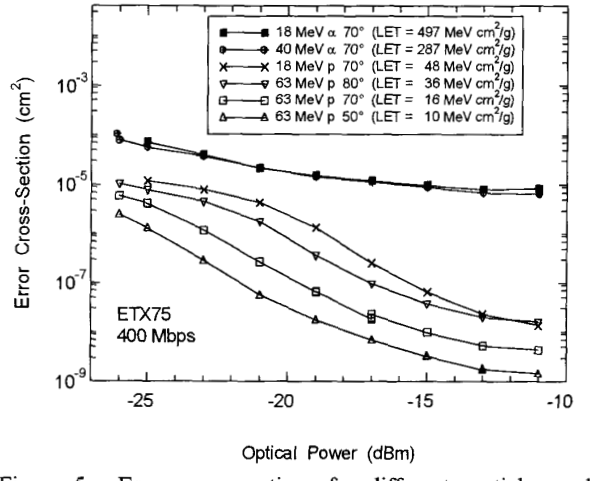

Figure 5. Error cross-sections for different particles and different angles identified with the particle's effective LET.

Further inspection of Figure 5 reveals the cross-section dependence on LET, shown as the vertical trend at a given optical power. Figure 6 shows this in more conventional terms as six separate data sets revealing the dependence of the cross-section versus LET dependence on optical power. Note that the LET units in the legend are MeV·cm²/g (and not per mg) consistent with sensitivities orders of magnitude below conventional soft RAM technologies, even at the higher optical powers. The solid curves paired with the data are fitted according to the cumulative Weibull distribution of equation (1) which apparently describes the LET dependence very nicely. The Table contains values for the variables at each of the six optical power levels. Note how c, the shape parameter, increases systematically with power. Also, the excellent fits at the lower LET values are obtained assuming a threshold of **zero!** Perhaps this is not so surprising in light of the

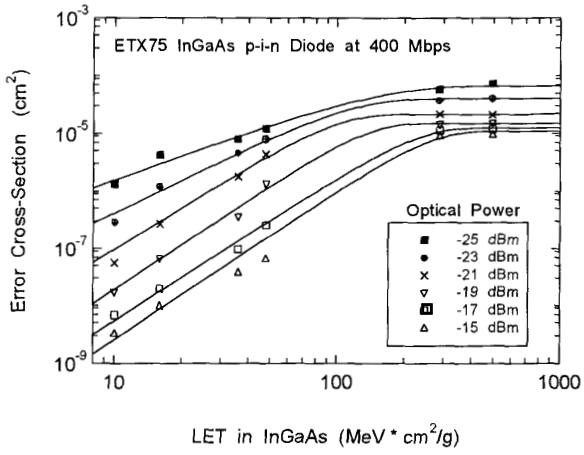

Figure 6. Weibull distributions accurately describe the cross-section with LET trends assuming a threshold LET of 0!

$$\sigma(LET) = \left[1 - e^{-\left(\frac{LET-a}{b}\right)^{c}}\right]\sigma_{sat} \quad (1)$$

Optical Power (dBm)	Weibull Parameters: LET_{th} -a-	Scale -b-	Shape -c-	Saturation Cross-section σ_{sat} (cm^2)
-25	0	145	1.4	6.7e-5
-23	0	110	1.9	4.0e-5
-21	0	85	2.7	2.15e-5
-19	0	130	2.6	1.5e-5
-17	0	220	2.5	1.25e-5
-15	0	250	2.6	1.1e-5

discussion of symbol detection probability in section II A. In fact, a zero threshold is predicted by our analytic model discussed in section VI.

C. BER Analysis

Having interpreted the cross-section dependence on LET and adapted the environmental models to the appropriate material and geometry as in section II B, the two can now be folded together exactly as with memory SEU analysis to predict the upset rate in orbit. To remain consistent with communications link analysis, we examine this in terms of BER, which can now be calculated as shown in equation (2). Results of these calculations for each optical power are presented in Figure 7 for the solar flare conditions shown in Figure 2. As a figure-of-merit, BER values greater than 10^{-9} are usually considered unacceptable, and from the figure we note that optical powers of > -23 dBm would be required to assure less than 10^{-9} BER under these flare conditions.

$$BER = \frac{\#errors}{Bits\_Transmitted} = \frac{\sigma \cdot \phi}{Data\_Rate} \quad (2)$$

To assess the BER dependence on data rate, we could analyze other data sets measured at other rates as we have for the 400 Mbps data set, however more general results can be obtained by inspecting Figure 8 which plots cross-section dependence on optical power for 200, 400, and 1000 Mbps. The two data sets shown represent the highest and lowest LET particles reported

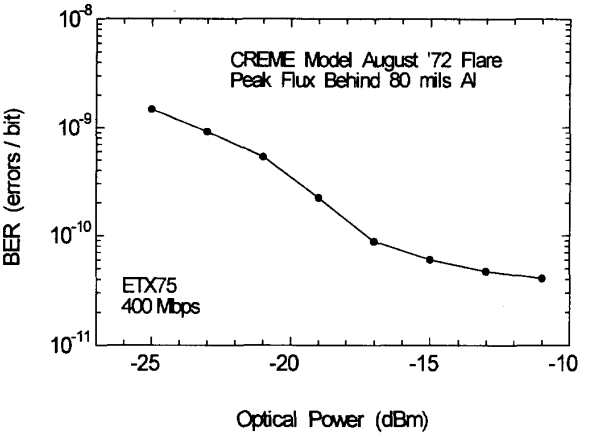

Figure 7. Flare particle induced errors result in bit error ratios over 10^{-9} and decrease sharply with increased power.

in our study. Note that across the full optical power range and for these two extremes in particle LET, the cross-section exhibits, to first order, a direct proportionality to data rate. This trend was noted in all of our data. According to equation 2, a cross-section which is proportional to data rate results in a BER which is *independent* of data rate. We would expect this result to hold *provided* the bandwidth of the receiver circuit remains unchanged.

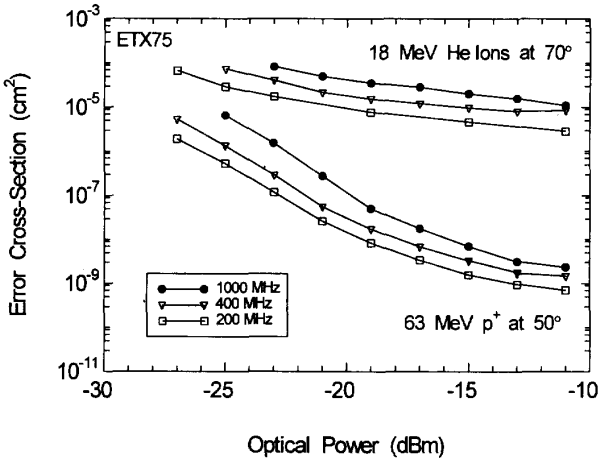

Figure 8. For the highest and lowest LET ions used in this study, the cross-section scales approximately with data rate.

V. BER Modeling and Discussion

Confirmation of the error cross-section dependence on particle LET enables flight predictions based on test data. In this section, we consider a completely analytic modeling approach to serve the following three purposes: first, to enable a comparison and sanity check with the semi-empirical approach already described;

next, to provide designers with an evaluation tool for candidate receiver implementations; and finally, to explore possible hardening approaches at both the component and circuit level.

Referring back to section II A and Figure 1, the model seeks to predict the likelihood that ion-induced photocurrent would exceed the circuit decision threshold when a "0" is being transmitted. For the link described in sections II and III, we know the current associated with a given average incident optical power, based on the rated diode quantum efficiency of 0.8 amps per watt of incident light. Also, the ratio of the high and low current levels, i_1 and i_0 in Figure 1, is approximately 10. This establishes the absolute difference between the average signal representing a "0" and the decision level, assuming the decision level is midway between the high and low signal levels. The distribution about the average signal representing a "0", referring back to Figure 1, is gaussian with a variance consistent with the expected error rate with no particles present. For example, at -27 dBm incident power, we expect (and we measure) a BER of 10^{-9} without particles. For this power, the appropriate gaussian has a variance corresponding to an area above the threshold of 5×10^{-10}. Similar arguments apply to the gaussian describing detection of "1s", though this is not usually an issue for particle induced effects. Note there are two important results from increasing the power while this variance remains constant. First, we see fewer errors without particles present (as expected), and second, the ion-induced pulse required to disrupt a bit increases, as we see reflected in the data. The gaussian distribution of signal levels suggests a distribution of critical charges for bit loss which extends to zero. Experimantal evidence for this appears in the table on the previous page.

The results of the CREME environment calculations, shown in Figure 2, determine the rate at which charges of given amounts will be deposited in the circuit. The model assumes these charges will arrive randomly in time and decay according to the RC time constant of the receiver circuit. Following the analysis first discussed in [4], we estimate our test circuit has an RC time constant of about 100 ps, and use this value to evaluate the probability that ion-induced photocurrent will exceed the decision level.

Model predictions are in qualitative agreement with the anticipated BER for flare conditions shown in Figure 7. Agreement is within a factor of 3 at powers below -19 dBm. At higher powers, the model does not predict the apparent flattening of the BER power dependence above -17 dBm. We offer two possible explanations. First, there may be some mechanism not accounted for in the model. We recognize that proton-induced reactions will play an increasingly important role as the increases in optical power mitigate the ionization effects. Referring back to Figure 4, we see that the 63 MeV proton cross-sections decrease over three orders of magnitude; then appear to flatten. Estimates of about 1 reaction in 10^4 protons in our structure suggests this may be a factor. It is interesting to see, in Figure 5, that the 18 MeV proton data decreases more rapidly at higher optical power levels than the corresponding data for 63 MeV protons where reactions would be more important.

The second explanation involves our test equipment's dynamic range. After the first high gain stage, 1000 V/amp, the signal is further boosted by an ECL limiting amplifier. Without particles incident, we saturate this amplifier at -9 dBm and can no longer operate the link. At slightly lower optical powers, this amplifier is driven into partial compression. This could lead to nonlinear behavior and over estimation of the error cross-section relative to the model.

In future experiments, attenuators will be placed ahead of the ECL stage for tests at the higher signal levels. This will enable BER measurements up to 0 dBm and allow us to rule out the circuit related explanation Also, this will allow us to firmly establish the role of reaction recoils.

We consider the model preliminary until it can be benchmarked against a variety of circuit variables encompassing a range of sensitivities and bandwidths. Even so, it has already served as a useful qualitative tool for understanding cross-section LET and optical power dependencies and for predicting the LET threshold of 0.

VI. Conclusions

We have demonstrated quantitative approaches to evaluate orbital particle effects on fiber optic receivers. Ion-induced bit error data from a range of proton and alpha particle angles and energies provide the basis for an analysis in terms of the particle LET. This parallels conventional heavy ion analysis but is modified to cover the case of temporally distributed bits. Taking this into

account, along with the materials issues (e.g. LET and ionization potential) for InGaAs detectors, we see that the tools developed for heavy ion analysis are appropriate for analysis of receiver bit errors, even though they are orders of magnitude more sensitive that conventional memory cells.

We have explored the ion-induced mechanisms which may affect the uncorrected BER. Both the empirical and analytic analyses reveal the importance of the incident optical power and circuit parameters to mitigate bit errors. Physical diode characteristics are also important, and small geometry direct bandgap detectors are recommended for satellite applications.

Data and analysis such as those described here are new and necessary to support development of design practices for fiber-based links in space radiation environments. While it is probably not practical to eliminate all particle-induced effects, we consider it possible to attain acceptable bus performance with minor constraints to the system design. Studies such as this are necessary so the many advantages of fiber based data links and busses can soon be made available for emerging satellite requirements to route data reliably at rates from a few Kbps into the Gbps regime.

VII. ACKNOWLEDGEMENTS

The authors wish to acknowledge helpful discussions with Julian Bristow, John Holm, Fred Orlando and Steve Rankin. We also thank DNA for partial support of this work.

VIII. REFERENCES

1. B.S. Smith, "SEDS Segment Specification for a MIL-STD-1773 Data Bus System for the Small Explorer Data System", NASA GSFC-730-89-011, 1990.
2. Anthony F. Jordan, "On the Brink: Fiber Optic LANs for Avionics and Space", Defense Electronics, Vol. 25, No. 11, pp. 43-47, 1993.
3. Michael de La Chapelle, Arthur W. Van Ausdale, and Martin E. Fritz, "The STAR-FODB (Fiber Optic Data Bus) Program", GOMAC 93 Conference Proceedings, p. 395.
4. Julian Bristow and John Lehman, "Component Tradeoffs and Technology Breakpoints for a 50 Mbps to 3.2 Gbps Fiber Optic Data Bus for Space Applications," Proc. SPIE, Vol. 1953, pp. 159-169, 1993.
5. John DeRuiter, "Survivable ring architecture for spaceborne applications", Proc. SPIE, Vol. 1953, pp. 128-135, 1993.
6. S. Gross, "ATM-Based Protocol for Gbps Ring Networks", GOMAC 93 Conference Proceedings, p. 399.
7. Kenneth A. LaBel, Paul Marshall, Cheryl Dale, Christina M. Crabtree, E.G. Stassinopolous, Jay T. Miller and Michele M. Gates, "SEDS MIL-STD-1773 Fiber Optic Data Bus: Proton Irradiation Test Results and Spaceflight SEU Data, IEEE Trans. Nucl. Sci. NS-40, (6), p. 1638 (1993).
8. Paul W. Marshall, Cheryl J. Dale, E. Joseph Friebele, and Kenneth A. LaBel, "Survivable Fiber-Based Data Links for Satellite Radiation Environments," SPIE Critical Review CR-14, Fiber Optics Reliability and Testing, (1994).
9. D.C. Meshel, G.K. Lum, P.W. Marshall, and C.J. Dale, "Proton Testing of InGaAsP Fiber Optic Transmitter and Receiver Modules," IEEE Radiation Effects Workshop Proceedings, NSREC (1994).
10. Paul Marshall, Cheryl Dale, and Ken LaBel, "Charged Particle Effects on Optoelectronic Devices and Bit Error Rate Measurements on 400 Mbps Fiber Based Data Links," RADECS Conference Proceedings, September 13-16, 1993, Saint Malo, France, pp. 266-71.
11. We used the CREME model as contained in the software package SPACE RADIATION®, Severn Comm. Corp., Millersville, MD. This version has been modified to correct integration errors encountered in the CREME model when evaluating sub-femptocoulomb charges.